

# Raman scattering from Higgs mode oscillations in the two-dimensional antiferromagnet $\text{Ca}_2\text{RuO}_4$

Sofia-Michaela Souliou,<sup>1,2</sup> Jiří Chaloupka,<sup>3,4</sup> Giniyat Khaliullin,<sup>1</sup> Gihun Ryu,<sup>1</sup>  
Anil Jain,<sup>1</sup> B. J. Kim,<sup>1</sup> Matthieu Le Tacon,<sup>1,5</sup> and Bernhard Keimer<sup>1</sup>

<sup>1</sup>Max Planck Institute for Solid State Research, Heisenbergstrasse 1, D-70569 Stuttgart, Germany

<sup>2</sup>European Synchrotron Radiation Facility, BP 220, F-38043 Grenoble Cedex, France

<sup>3</sup>Central European Institute of Technology, Masaryk University, Kamenice 753/5, 62500 Brno, Czech Republic

<sup>4</sup>Department of Condensed Matter Physics, Faculty of Science,  
Masaryk University, Kotlářská 2, 61137 Brno, Czech Republic

<sup>5</sup>Karlsruhe Institute of Technology, Institut für Festkörperphysik, D-76021 Karlsruhe, Germany

(Dated: July 13, 2017)

We present and analyze Raman spectra of the Mott insulator  $\text{Ca}_2\text{RuO}_4$ , whose quasi-two-dimensional antiferromagnetic order has been described as a condensate of low-lying spin-orbit excitons with angular momentum  $J_{\text{eff}} = 1$ . In the  $A_g$  polarization geometry, the amplitude (Higgs) mode of the spin-orbit condensate is directly probed in the scalar channel, thus avoiding infrared-singular magnon contributions. In the  $B_{1g}$  geometry, we observe a single-magnon peak as well as two-magnon and two-Higgs excitations. Model calculations using exact diagonalization quantitatively agree with the observations. Together with recent neutron scattering data, our study provides strong evidence for excitonic magnetism in  $\text{Ca}_2\text{RuO}_4$  and points out new perspectives for research on the Higgs mode in two dimensions.

PACS numbers: 75.10.Jm

The notion of Goldstone and Higgs modes, corresponding to phase and amplitude oscillations of a condensate of quantum particles, appears in many areas of physics including magnetism [1]. In quantum magnets, especially near quantum criticality [2], the magnetization density is far from being saturated and hence allowed to oscillate near its mean value, forming a collective amplitude mode.

The “magnetic” Higgs mode has been observed [3] in quantum dimer systems, where the magnetic order is due to Bose-Einstein condensation of spin-triplet excitations [4]. A conceptually similar, but physically distinct case is expected in Van Vleck-type Mott insulators, where the “soft” moments result from condensation of spin-orbit excitons [5], that is, magnetic transitions between spin-orbit  $J_{\text{eff}} = 0$  and  $J_{\text{eff}} = 1$  levels propagating via exchange interactions. Recent inelastic neutron scattering (INS) experiments [6] on  $\text{Ca}_2\text{RuO}_4$  have indeed revealed Higgs oscillations of the magnetization in this material, which is based on nominally non-magnetic, spin-orbit singlet  $\text{Ru}^{4+}$  ions. A detailed analysis of the dispersion relations of the Higgs mode and magnons determined by INS showed that  $\text{Ca}_2\text{RuO}_4$  is close to a quantum critical point associated with the condensation of  $J_{\text{eff}} = 1$  excitons [6].

The unique aspect of  $\text{Ca}_2\text{RuO}_4$  is that it hosts Higgs physics in a two-dimensional setting, which has been a focus of many theoretical studies [7–15]. As the magnetization density is not a conserved quantity, the Higgs mode is not symmetry protected, and various decay processes convert it into a many-body resonance with  $\sim \omega^3$  onset. It was also emphasized [7] that the actual appearance of this resonance strongly depends on the symme-

try of the probe. In INS experiments, which probe the longitudinal magnetic susceptibility, the low-energy behaviour of the Higgs resonance is masked by the infrared-singular two-magnon contribution. To avoid contamination by the Goldstone modes, the probe should couple to the condensate in the scalar channel (i.e. insensitively to the phase/direction). Precisely this type of experiment has been done in ultracold atomic systems [16].

In this Letter, we demonstrate that Raman light scattering in the fully symmetric, i.e.  $A_g$  channel can serve as a scalar probe in magnetic systems, thus providing direct access to Higgs oscillations of “soft” moments. While in conventional Heisenberg magnets with rigid spins (such as  $\text{La}_2\text{CuO}_4$  or  $\text{Sr}_2\text{IrO}_4$ ) the  $A_g$  channel is magnetically silent, the size of the local moments, and hence the magnetization density in excitonic systems is determined by a balance between the spin-orbit  $\lambda$  and exchange  $J$ -interactions [5, 6], and the  $A_g$  modulation of the latter directly shakes the condensate density.

The Raman scattering data in  $\text{Ca}_2\text{RuO}_4$  presented below indeed reveal a pronounced magnetic contribution in the  $A_g$  channel, which we identify and describe using the same excitonic model that has already been parameterized in the INS study [6]. In the  $B_{1g}$  channel, we observe the expected two-magnon scattering and an additional two-Higgs scattering contribution, as well as a single-magnon peak. All the observations are coherently explained by model calculations.

*Experiment.*—Single crystals of  $\text{Ca}_2\text{RuO}_4$  with  $T_N = 110$  K were grown by a floating zone method, as described elsewhere [17]. The Raman data were recorded

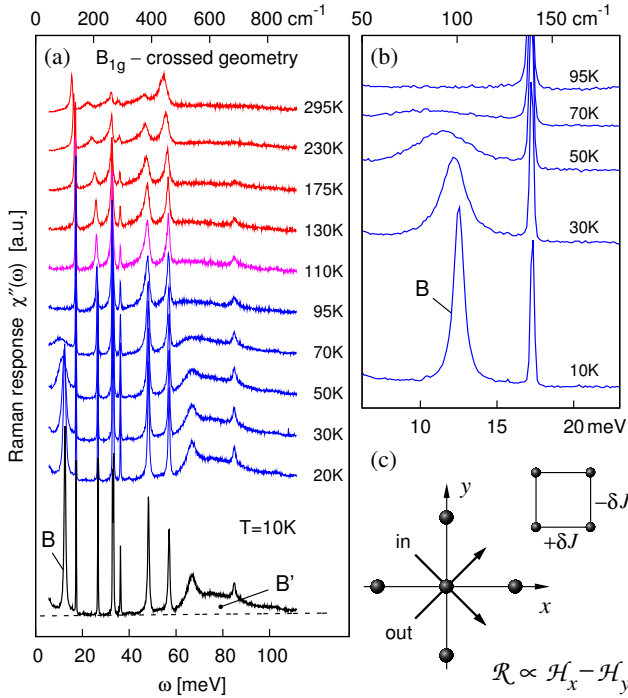


FIG. 1. (a) Raman spectra in  $B_{1g}$  scattering geometry with two magnetic features  $B$ ,  $B'$  appearing below  $T_N$ . The background (dashed line) is subtracted in further analysis. (b) Detailed view on the feature  $B$ . (c) Polarization vectors of incoming and outgoing photons with respect to the Ru lattice. In the Raman process, the exchange is modulated with opposite signs on  $x$  and  $y$  bonds leading to the Raman operator  $\mathcal{R} \propto \mathcal{H}_x - \mathcal{H}_y$ .

on a Labram (Horiba Jobin-Yvon) single-grating Raman spectrometer, using the 632.817 nm line of a  $\text{He}^+/\text{Ne}^+$  mixed gas laser. The experiments were performed in backscattering geometry along the crystallographic  $c$ -axis.  $\text{Ca}_2\text{RuO}_4$  crystallizes in the orthorhombic  $Pbca-D_{2h}^{15}$  space group. Excitations in the  $B_{1g}$  and  $A_g$  representations of the point group  $D_{2h}$  were probed in crossed and parallel configurations respectively, with the polarization of the incident light at  $45^\circ$  to the Ru-Ru bonds [see Figs. 1(c) and 2(c)]. The spectra were corrected for the Bose thermal factor to obtain the Raman response functions  $\chi''(\omega)$ .

Temperature-dependent  $\chi''(\omega)$  in the range of 5 to 110 meV are plotted in Figs. 1 and 2. The frequencies of the observed phonon modes are in good agreement with previous Raman studies [18]. The phonon modes are superimposed on top of a broad continuum. As the temperature is lowered, the continuum evolves into distinct spectral features  $B$ ,  $B'$  (Fig. 1) and  $A$ ,  $A'$  (Fig. 2). The temperature dependence of the new features follows closely that of the magnetic order parameter and strongly suggests their magnetic origin. The fact that these excitations are well inside the optical gap exceeding 0.5 eV [19] further supports this interpretation.

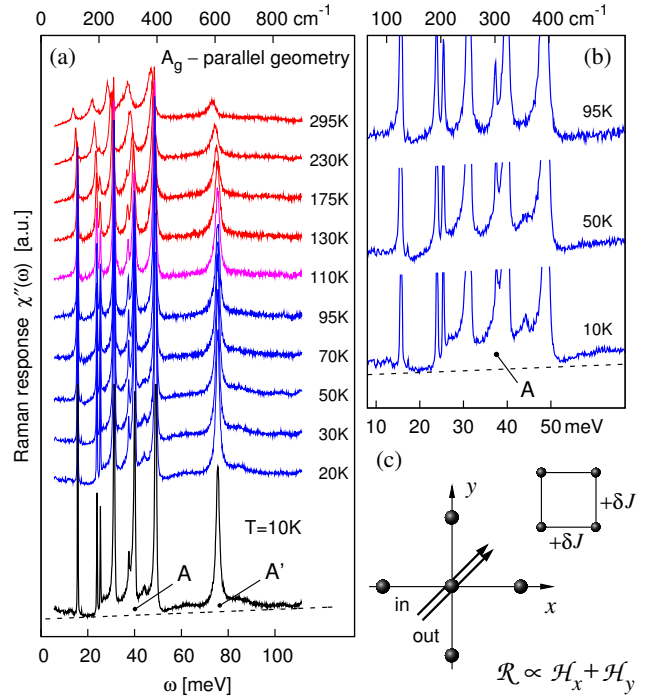


FIG. 2. (a) Raman spectra in  $A_g$  scattering geometry with two magnetic features  $A$ ,  $A'$  appearing below  $T_N$ . (b) Detailed view on the feature  $A$ . (c) The polarization vectors in the  $A_g$  setup. In this case, the exchange is modulated equally on  $x$  and  $y$  bonds and the Raman operator  $\mathcal{R} \propto \mathcal{H}_x + \mathcal{H}_y$ .

More specifically, in the  $B_{1g}$  channel, the feature  $B$  appears around 12 meV and gradually sharpens [Fig. 1(b)]. Earlier Raman studies attributed it either to two-magnon scattering [20, 21] or to a zone-boundary folded phonon in the magnetically ordered state [18]. However, we find below that the two-magnon scattering is represented by the  $B'$  structure around 80 meV, while the  $B$ -peak is identified as a single-magnon excitation.

In the  $A_g$  channel, the  $A$ -structure in the range of 25 to 50 meV develops in the magnetically ordered state [Fig. 2(b)]. The phonon modes in this spectral region exhibit pronounced Fano-type asymmetric lineshapes – a clear signature of the presence of a continuum of excitations coupled to the phonons. As noticed above, the large optical gap implies a magnetic origin of the continuum.

*Extraction of the magnetic response.*—We adopt the Green's function approach [22–24] to the Raman response of the coupled system of phonons and a continuum. We describe the system by a matrix propagator whose inverse  $G^{-1}(\omega)$  contains the response functions of the magnetic  $[G^{-1}(\omega)]_{00} = R(\omega) + iS(\omega)$  and phonon  $[G^{-1}(\omega)]_{mn} = \omega_n - \omega - i\Gamma_n$  ( $n = 1 \dots N$ ) subsystems as the diagonal elements. The coupling between phonon  $n$  and the continuum is provided by nondiagonal matrix elements  $[G^{-1}(\omega)]_{n0} = [G^{-1}(\omega)]_{0n} = V_n$ . After inverting  $G^{-1}(\omega)$ , the Raman response is obtained as  $\chi''(\omega) =$

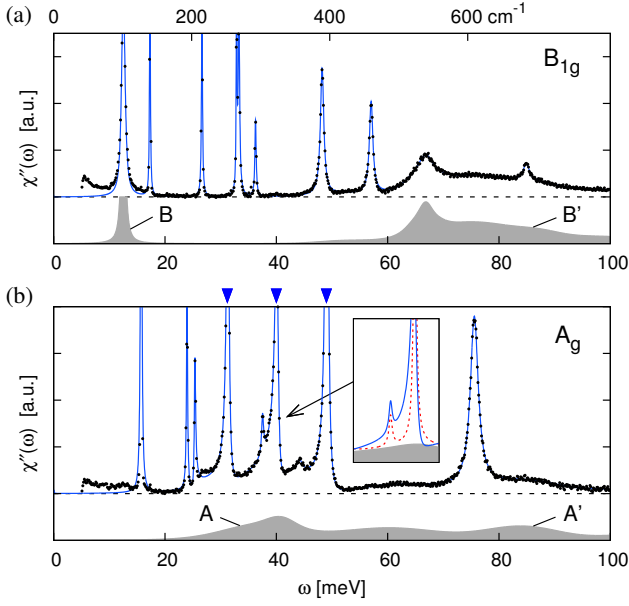


FIG. 3. Fits of  $T = 10$  K Raman spectra in  $B_{1g}$  (a) and  $A_g$  (b) channels using a model of phonons interacting with a magnetic continuum. The model response (blue) is compared to the experimental points (black). The obtained magnetic signal  $S(\omega)$  is indicated by shading. The  $A_g$  phonons marked by blue triangles are most strongly affected by the spin-phonon interaction which changes their lineshape dramatically, compared to the non-interacting case (red dashed line in the inset). The associated spectral-weight transfer is moderate only.

$\sum_{j=0}^N W_j [\text{Im } G(\omega)]_{jj}$ , where  $W_j$  are spectral weights of the normal modes of the coupled spin-phonon system.

The magnetic response functions  $S(\omega)$ , determined by fitting  $\chi''(\omega)$  to the low-temperature spectra, are presented in Fig. 3. While in the  $B_{1g}$  case the above procedure just confirms the expected result, in the  $A_g$  case it proved essential to obtain the actual  $S(\omega)$  profile. The feature A is found to be peaked at about 40 meV and has a long tail that merges with the high-energy continuum ( $A'$ ), much flatter than the  $B_{1g}$  one ( $B'$ ).

**Magnetic model.**—In the following, we give a quantitative interpretation of the magnetic features using the excitonic model of Ref. [5], refined further by a comparison to INS data [6]. The model utilizes the local basis depicted in Fig. 4(b) stabilized by intraionic spin-orbit coupling. The dominant energy scale corresponds to the energy cost  $E_T$  of a triplon  $T$  (derived from  $J_{\text{eff}} = 1$  states) relative to that of the singlet ground state  $s$  ( $J_{\text{eff}} = 0$ ). Its competition with the spin-orbital exchange interaction results in a quantum critical point separating the paramagnetic phase (dilute “gas” of  $T$  on top of  $s$  background) and antiferromagnetic phase (condensate with coherently mixed  $T$  and  $s$ ). In terms of hardcore bosons  $s$  and  $T_{x/y}$  associated with the relevant low-energy levels and obeying local constraint  $n_s + n_T = 1$ , these main constituents of the model

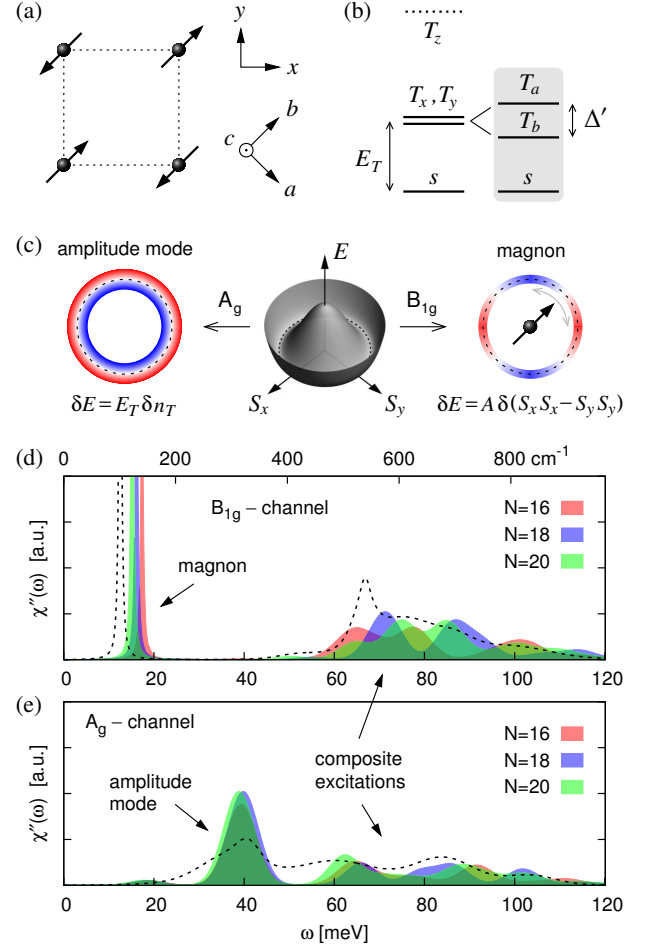


FIG. 4. (a) Coordinate frames for the Ru lattice. The ordered moments point along the  $b$  axis. (b) Multiplet structure of  $\text{Ru}^{4+}$  ions with groundstate singlet  $s$  with  $J_{\text{eff}} = 0$  and higher-lying magnetic states derived from  $J_{\text{eff}} = 1$  triplet. A tetragonal crystal field removes the degeneracy of the triplet states  $T$  by lifting up  $T_z$  [6]. An orthorhombic distortion further splits  $T_{x/y}$  into  $T_{a/b} = \frac{1}{\sqrt{2}}(T_x \mp T_y)$  levels forming together with  $s$  the basis for the low-energy model (shaded). (c) Modulation of the condensate energy (Mexican-hat potential) in the Raman process leading to an excitation of the amplitude mode ( $A_g$  channel). Note that  $\delta n_T \equiv \delta(S_x^2 + S_y^2)$ , i.e. the  $A_g$ -coupling is rotationally invariant. In contrast, the  $B_{1g}$ -coupling leads to the shape deformations, leaving condensate density intact. A single magnon is excited instead of the amplitude mode. (d),(e) Raman spectra obtained by exact diagonalization on clusters with  $N = 16, 18$ , and  $20$  sites [25] using  $E_T = 31$  meV,  $J = 7.5$  meV,  $A = 2.3$  meV,  $\alpha = 0.15$ , and  $\Delta' = 4$  meV. The ED data for  $B_{1g}$  (a) and  $A_g$  (b) channels are presented in identical scales and overlaid by the magnetic  $S(\omega)$  from Fig. 3(a),(b) (dashed).

are expressed as

$$\mathcal{H} = E_T \sum_i n_{T_i} + J \sum_{\langle ij \rangle, \gamma=x,y} (T_{\gamma i}^\dagger s_i s_j^\dagger T_{\gamma j} - T_{\gamma i}^\dagger s_i T_{\gamma j}^\dagger s_j + \text{H.c.}). \quad (1)$$

The exchange interaction  $J$  comprises triplon hopping

and pair creation/annihilation which act together to form AF-aligned pairs of Van Vleck moments.

The full model is most conveniently expressed using pseudospin  $S=1$  formed by the three levels  $\{s, T_x, T_y\}$  [6]. The corresponding in-plane operators  $S_\gamma = -i(s^\dagger T_\gamma - T_\gamma^\dagger s)$  for  $\gamma = x, y$  are directly linked to the dominating Van Vleck part of magnetic moment, while  $S_z = -i(T_x^\dagger T_y - T_y^\dagger T_x)$  is related to the moment residing in the excited  $T$  levels. In this basis, the  $J$ -term in Eq. (1) takes a form of the XY-model  $J(S_i^x S_j^x + S_i^y S_j^y)$ . Supplemented by the bond-directional interaction  $A$  and coupling between the out-of-plane  $S_z$  components, the exchange Hamiltonian for the  $x$ -bonds reads as

$$\mathcal{H}_x = \sum_{\langle ij \rangle \parallel x} \left[ (J+A) S_i^x S_j^x + (J-A) S_i^y S_j^y + J(1-\alpha) S_i^z S_j^z \right]. \quad (2)$$

The signs of the  $A$  terms are opposite for  $y$  bonds. The  $T_{x/y}$ -level orthorhombic splitting [see Fig. 4(a),(b)] orienting the moments along  $b$  axis translates into a single-ion anisotropy  $\mathcal{H}_{\Delta'} = -\Delta'(S_x S_y + S_y S_x) = \frac{1}{2} \Delta' (S_a^2 - S_b^2)$ . The full Hamiltonian used below is then  $\mathcal{H} = E_T n_T + \mathcal{H}_x + \mathcal{H}_y + \mathcal{H}_{\Delta'}$ , with  $n_T = S_z^2$ .

*Model calculations and interpretation of the data.*—We employ the Loudon-Fleury [26] Raman scattering operator  $\mathcal{R} \propto \sum_{\langle ij \rangle} (\epsilon_{\text{in}} \cdot \mathbf{r}_{ij})(\epsilon_{\text{out}} \cdot \mathbf{r}_{ij}) \mathcal{H}_{ij}$ , which modulates the exchange interactions  $\mathcal{H}_{ij}$  in a way determined by the incoming  $\epsilon_{\text{in}}$  and outgoing  $\epsilon_{\text{out}}$  polarization vectors [27]. Specifying  $\epsilon_{\text{in}}$  ( $\epsilon_{\text{out}}$ ) by its angle  $\varphi$  ( $\varphi'$ ) to the  $a$  axis,  $\mathcal{R}$  becomes

$$\mathcal{R} \propto \cos(\varphi - \varphi') (\mathcal{H}_x + \mathcal{H}_y) + \sin(\varphi + \varphi') (\mathcal{H}_x - \mathcal{H}_y). \quad (3)$$

For  $B_{1g}$  ( $\varphi = 0, \varphi' = \pi/2$ ) and  $A_g$  ( $\varphi = \varphi' = \pi/2$ ) symmetries, only the  $\mathcal{H}_x - \mathcal{H}_y$  or  $\mathcal{H}_x + \mathcal{H}_y$  term above is active, respectively.

We first discuss the implications of Eq. (3) on a qualitative level. Consider the  $A_g$  scattering channel with  $\mathcal{R} \propto \mathcal{H}_x + \mathcal{H}_y$ . While in the usual rigid spin systems (e.g. cuprates) this operator is proportional to the Hamiltonian itself and does not bring any dynamics, here we may replace it by its complement in the Hamiltonian, i.e.  $\mathcal{R} \propto E_T n_T$  (and a small  $\Delta'$  term), and obtain a non-trivial spectrum. Most importantly,  $E_T n_T$  globally changes the balance between the  $s$  and  $T_{x/y}$  components coherently mixed in the condensate, exciting thus directly the amplitude mode of the condensate. This  $A_g$  Raman process may be intuitively understood as a forced expansion and contraction of the Mexican-hat potential in Fig. 4(c). In contrast to INS, the amplitude mode is probed here in a rotationally invariant way, using a scalar coupling to the condensate density. We thus avoid the contamination by the two-magnon response that leads to a drastic broadening of the longitudinal mode in the dynamical spin susceptibility.

In the  $B_{1g}$  channel, the modulation of the exchange  $J$  contained in  $\mathcal{R} \propto \mathcal{H}_x - \mathcal{H}_y$  produces a high-energy two-magnon continuum, as in usual Heisenberg magnets. Here it is additionally supported by other composite excitations such as two-Higgs continuum (similar to what found in a soft-spin model [28]). A special role is played by the bond-anisotropic  $A$  term contributing to  $\mathcal{R}$  as  $A \sum_{\langle ij \rangle} (S_i^x S_j^x - S_i^y S_j^y)$ . The resulting quadrupolar modulation of the condensate energy [see Fig. 4(c)] drives the ordered moment toward the  $x$  or  $y$  directions hence exciting a magnon.

To confirm the above expectations and make a quantitative comparison to the experiment, in Fig. 4(d),(e) we show Raman spectra calculated by exact diagonalization (ED). The best fit to the magnetic intensity extracted in Fig. 3 is obtained for the parameters  $E_T = 31$  meV,  $J = 7.5$  meV,  $A = 2.3$  meV,  $\alpha = 0.15$ , and  $\Delta' = 4$  meV, well matching those from the INS data [6]. The small differences in  $E_T$  and  $J$  is due to the different methods – the spin-wave approach [6] versus ED used here.

In accord with the above discussion, the  $B_{1g}$  model spectrum in Fig. 4(d) contains a high-energy continuum and a single-magnon peak due to the bond-directional  $A$ -part of  $\mathcal{R}$  that sums up to  $A \sum_{\langle ij \rangle} (S_i^a S_j^b + S_i^b S_j^a)$ . Approximating  $S$  along the ordered moment direction by  $S_{\mathbf{R}}^b \approx \langle S_{\parallel} \rangle e^{i\mathbf{Q} \cdot \mathbf{R}}$  with  $\mathbf{Q} = (\pi, \pi)$ , this part becomes  $A \langle S_{\parallel} \rangle S_{\mathbf{Q}}^a$  thus probing the magnon at the ordering vector. The energy of the experimental feature  $B$  of about 12.5 meV indeed agrees with that of INS  $(\pi, \pi)$ -magnon peak [6, 29]. The spectral weight (SW) of the peak  $B$  is roughly proportional to  $A^2$ , enabling us to estimate  $A$  by comparing the SW of  $B$  and that of the  $B'$  continuum. The experimental SW ratio obtained from Fig. 3(a) amounts to 0.27. In the model calculations, the average through the three clusters gives a consistent value of 0.30, confirming  $A \simeq 2.3$  meV taken from INS fits.

In the  $A_g$  channel, the model spectrum in Fig. 4(e) is dominated by the amplitude mode appearing at 40 meV in agreement with the expected position of the bare amplitude mode based on INS (see Fig. 4 of Ref. [6]). The amplitude mode peak is accompanied by a high-energy continuum [Fig. 4(e)]. Since it is a part of the  $n_T$  susceptibility, its profile is rather different than that of the (mainly) two-magnon continuum in the  $B_{1g}$  channel. The limited scattering possibilities on the small clusters do not allow us to access the mode profile by ED in detail. The available results for the relativistic quantum  $O(N)$  model in  $2 + 1$  dimensions [11–14] suggest a Higgs peak with  $\sim \omega^3$  onset and an extended tail which is in a qualitative agreement with  $S(\omega)$  extracted in Fig. 3(b).

Finally, we comment on the notable interplay of phonons with the amplitude mode observed in Fig. 3(b). First,  $A_g$  phonons involving rotations and tiltings of  $\text{RuO}_6$  octahedra modify the Ru-O-Ru bond angle, thus modulat-

ing the exchange  $J$  in a symmetric fashion. Second, deformations of the octahedra affect the splitting among  $t_{2g}$  orbitals, thus modulating  $E_T$  owing to the different orbital composition of  $s$  and  $T_{xy}$  states. Both mechanisms provide a natural coupling of phonons to oscillations of the condensate density that is determined by the ratio  $E_T/J$ .

In conclusion, we have presented Raman light scattering data on  $\text{Ca}_2\text{RuO}_4$  and fully interpreted its magnetic features in terms of the excitonic model [5, 6]. As demonstrated, the  $A_g$  scattering channel enables direct access to the amplitude (Higgs) mode of the spin-orbit condensate. In contrast to INS, the Higgs mode is probed here via a scalar coupling and is not obscured by the two-magnon continuum. The overall agreement with both the neutron and Raman experiments strongly supports the excitonic picture as the basis for magnetism of  $\text{Ca}_2\text{RuO}_4$ . More generally, our results encourage future experimental efforts to explore other compounds based on Van Vleck-type ions such as  $\text{Ru}^{4+}$ ,  $\text{Os}^{4+}$ , and  $\text{Ir}^{5+}$ .

JC acknowledges support by the Czech Science Foundation (GAČR) under Project No. GJ15-14523Y and MŠMT ČR under NPU II project CEITEC 2020 (LQ1601). BK acknowledges support by the European Research Council under Advanced Grant 669550 (Com4Com) and by the German Science Foundation (DFG) under the coordinated research program SFB-TRR80.

- 
- [1] D. Pekker and C. M. Varma, *Annu. Rev. Condens. Matter Phys.* **6**, 269 (2015).
  - [2] S. Sachdev and B. Keimer, *Phys. Today* **64**, 29 (2011).
  - [3] Ch. Rüegg, B. Normand, M. Matsumoto, A. Furrer, D. F. McMorrow, K. W. Krämer, H.-U. Güdel, S. N. Gvasaliya, H. Mutka, and M. Boehm, *Phys. Rev. Lett.* **100**, 205701 (2008).
  - [4] T. Giamarchi, Ch. Rüegg, and O. Tchernyshyov, *Nature Phys.* **4**, 198 (2008).
  - [5] G. Khaliullin, *Phys. Rev. Lett.* **111**, 197201 (2013).
  - [6] A. Jain, M. Krautloher, J. Porras, G. H. Ryu, D. P. Chen, D. L. Abernathy, J. T. Park, A. Ivanov, J. Chaloupka, G. Khaliullin, B. Keimer, and B. J. Kim, *Nature Phys.* **13**, 633 (2017).
  - [7] D. Podolsky, A. Auerbach, and D. P. Arovas, *Phys. Rev. B* **84**, 174522 (2011).
  - [8] D. Podolsky and S. Sachdev, *Phys. Rev. B* **86**, 054508 (2012).
  - [9] L. Pollet and N. Prokof'ev, *Phys. Rev. Lett.* **109**, 010401 (2012).
  - [10] K. Chen, L. Liu, Y. Deng, L. Pollet, and N. Prokof'ev, *Phys. Rev. Lett.* **110**, 170403 (2013).
  - [11] S. Gazit, D. Podolsky, and A. Auerbach, *Phys. Rev. Lett.* **110**, 140401 (2013).
  - [12] S. Gazit, D. Podolsky, A. Auerbach, and D. P. Arovas, *Phys. Rev. B* **88**, 235108 (2013).
  - [13] A. Rançon and N. Dupuis, *Phys. Rev. B* **89**, 180501(R) (2014).
  - [14] F. Rose, F. Léonard, and N. Dupuis, *Phys. Rev. B* **91**, 224501 (2015).
  - [15] Y. T. Katan and D. Podolsky, *Phys. Rev. B* **91**, 075132 (2015).
  - [16] M. Endres, T. Fukuhara, D. Pekker, M. Cheneau, P. Schauß, Ch. Gross, E. Demler, S. Kuhr, and I. Bloch, *Nature* **487**, 454 (2012).
  - [17] S. Nakatsuji and Y. Maeno, *J. Solid State Chem.* **156**, 26 (2001).
  - [18] H. Rho, S. L. Cooper, S. Nakatsuji, H. Fukazawa, and Y. Maeno, *Phys. Rev. B* **71**, 245121 (2005).
  - [19] J. H. Jung, Z. Fang, J. P. He, Y. Kaneko, Y. Okimoto, and Y. Tokura, *Phys. Rev. Lett.* **91**, 056403 (2003).
  - [20] C. S. Snow, S. L. Cooper, G. Cao, J. E. Crow, H. Fukazawa, S. Nakatsuji, and Y. Maeno, *Phys. Rev. Lett.* **89**, 226401 (2002).
  - [21] H. Rho, S. L. Cooper, S. Nakatsuji, H. Fukazawa, and Y. Maeno, *Phys. Rev. B* **68**, 100404(R) (2003).
  - [22] A. Nitzan, *Mol. Phys.* **27**, 65 (1974).
  - [23] M. V. Klein, in *Light Scattering in Solids*, edited by M. Cardona (Springer-Verlag, Heidelberg, 1975).
  - [24] X. K. Chen, E. Altendorf, J. C. Irwin, R. Liang, and W. N. Hardy, *Phys. Rev. B* **48**, 10530 (1993).
  - [25] Clusters 16A, 18A, and 20A from D. D. Betts, H. Q. Lin, and J. S. Flynn, *Can. J. Phys.* **77**, 353 (1999) were used. The spectra were broadened by gaussians (FWHM=8meV), apart from the low-energy  $B_{1g}$  peak whose lineshape is taken from the  $B$  feature in Fig. 3(a).
  - [26] P. A. Fleury and R. Loudon, *Phys. Rev.* **166**, 514 (1968).
  - [27] Note that a direct excitation of the magnetic continuum requires  $\epsilon_{\text{in}}$  and  $\epsilon_{\text{out}}$  to be in the  $xy$ -plane. We have verified that the feature  $A$  and the associated Fano asymmetries are indeed absent in the  $zz$ -polarized Raman spectra (not shown).
  - [28] S. A. Weidinger and W. Zwerger, *Eur. Phys. J. B* **88**, 237 (2015).
  - [29] S. Kunkemöller, D. Khomskii, P. Steffens, A. Piovano, A. A. Nugroho, and M. Braden, *Phys. Rev. Lett.* **115**, 247201 (2015).